Monthly Notices
of the
ROYAL ASTRONOMICAL SOCIETY

MNRAS **474,** 1752–1761 (2018)
Advance Access publication 2017 November 13

doi:10.1093/mnras/stx2902

Relativistic R-matrix calculations for photoionization cross-sections of C IV: implications for photorecombination of C V

Shahid Sardar,[1,2]★ Xin Xu,[1,2] Long-Quan Xu[1,2]★ and Lin-Fan Zhu[1,2]★

[1]*Hefei National Laboratory for Physical Sciences at Micro-scale, Department of Modern Physics, University of Science and Technology of China, Hefei, Anhui 230026, People's Republic of China*
[2]*Synergetic Innovation Center of Quantum Information and Quantum Physics, University of Science and Technology of China, Hefei, Anhui 230026, People's Republic of China*

Accepted 2017 November 2. Received 2017 October 29; in original form 2017 July 9

ABSTRACT

In this paper we present photoionization cross-sections of the ground and excited states of Li-like carbon (C IV) in the framework of fully relativistic R-matrix formalism as implemented in Dirac atomic R-matrix code. For target wavefunctions expansion, Multiconfiguration Dirac Hartree Fock calculations are performed for the lowest 17 target states of He-like carbon (C V) arising from $1s^2$ and $1snl$, with $n = 2$, 3 and $l =$ s, p, d configurations. Our target energy levels and transition parameters belonging to these levels are ascertained to be in excellent agreement with the experimental and the well-established theoretical results. We use the principle of detailed balance to get the photorecombination (PR) cross-sections of the ground state of C V. Both photoionization and PR cross-sections manifest important KLL and KLM resonance structures which are in very good agreement with the accurate measurements at Advanced Light Source (ion photon end beam station) and CRYRING (synchrotron storage ring).

Key words: atomic data – atomic processes – methods: numerical – X-rays: general.

1 INTRODUCTION

Photoionization (PI) and its time inverse photorecombination (PR) are important charge changing processes which play a vital role for the study of X-ray astronomy. PI process is an important factor for determining the ionization balance in astrophysical sources like X-ray binary systems, cataclysmic variables, active galactic nuclei (AGNs) etc. (Kallman & Palmeri 2007), whereas, the ionization balance in high-temperature plasma environments is effected by the PR process which serves as a cooling mechanism. PR process also has a significant influence on the distribution of excited states of astronomical plasma like solar corona (Zhao, Ichihara & Shirai 2000). The new generation X-ray satellites *XMM–Newton* and *Chandra* provide highly resolved X-ray spectra which originate from many astronomical objects (Müller et al. 2009). Hence, the importance of understanding and testing the PI and PR calculation techniques has increased. Moreover, there is also a continuous development at the laboratory scale to measure these fundamental atomic processes. The ion-photon merged beams technique at Advanced Light Sources (Scully et al. 2006; Müller et al. 2009) and electron beam ion trap techniques are the manifestations of laboratory scale development. Therefore, it is essential to establish a connection between theory and experiment to benchmark the existing experimental techniques and theoretical atomic models (Ferland et al. 1998).

Carbon is among the elements which are the most abundant in the Universe and Solar system after hydrogen and helium. The K-shell transitions in C V lie in the soft X-ray region (Dere et al. 2001) and therefore C V is of prominent importance in the X-ray astronomy. Particularly its resonance lines ($1s^2\ ^1S_0 \rightarrow 1s2p\ ^1P^o_1$, $1s^2\ ^1S_0 \rightarrow 1s2p\ ^3P^o_{2,1}$, $1s^2\ ^1S_0 \rightarrow 1s2s\ ^3S_1$) play an important role in solar plasma diagnostics (Aggarwal et al. 2011). The absorption lines of the C IV are helpful for the investigation of the enrichment level in the intergalactic medium (Cooksey et al. 2010). The ionization stages of carbon can be used for solar wind diagnostics (Landi et al. 2012). It is also a very important component of interstellar medium (Sofia et al. 1997) and its Li-like ion is a key tracer in interstellar medium (Nahar, Pradhan & Zhang 2000). Besides the astrophysical applications, carbon has its crucial role in the fusion devices like Large Helical Device where it can be used as impurity pellet to achieve high-temperature ion plasma (Osakabe et al. 2014).

The astrophysical importance of carbon ions results in considerable amount of research works both on theoretical and experimental front. The dual laser plasma technique was used by Jannitti et al. (1995) to measure PI cross-sections of C IV for the first time. Müller et al. (2009) measured the PI cross-sections for ground state of C IV with a high spectral resolution by using the third-generation synchrotron radiation facility, Advanced Light Source (ALS). In order

★ E-mail: shahidpeace@gmail.com (SS); xuxin09@mail.ustc.edu.cn (L-QX); lfzhu@ustc.edu.cn (L-FZ)

to benchmark the experimental finding, they also performed theoretical calculations by using the semirelativistic R-matrix techniques (Berrington, Eissner & Norrington 1995; Robicheaux et al. 1995). Mannervik et al. (1997) measured the energies of doubly excited states of C IV from the PR spectrum of synchrotron-storage ring facility named CRYRING. Later PR cross-sections of C V were calculated by Zhao et al. (2000) in the rigorous theoretical treatment of continuum bound transitions. The Breit–Pauli R-matrix intermediate coupling approximations were carried out by Nahar et al. (2000) to obtain recombination rate coefficients for C V and C IV ions. These PI calculations for C IV are confined to R-matrix approach in LS coupling or in intermediate coupling scheme (Berrington et al. 1995). The effects of radiation damping (RD) on the resonances were also taken into the account in the previous theoretical works. However, instead of adding the spin–orbit interaction to the non-relativistic Hamiltonian, the R-matrix scheme can be further extended to fully relativistic Dirac formalism (Chang 1977; Norrington & Grant 1981). In the present study, without inclusion of RD, we aim to utilize this R-matrix scheme which is programmed as DARC (Dirac atomic R-matrix code) by P. H. Norrington and I. P. Grant to analyse the resonant cross-sections of C IV. Since the DARC code is based on *jj* coupling, it is likely to get higher accuracy in PI cross-sections for transitions among the fine structure levels.

In the R-matrix formalism of PI and PR cross-sections the atomic structure calculations are very crucial because the accuracy of these two processes depends on the better description of atomic states of residual or target ions. Here in the present study of PI cross-sections of C IV, the atomic structure calculations of C V consist of energy levels, transition energies, transition rates, oscillator strengths etc. The accuracy of these quantities will guaranty the correctness of the target description. He-like C is the simplest many electron system for the assessment of experimental and theoretical developments. Based on beam foil technique along with observations at JET tokamak, Engström et al. (1992) reported experimental energy level scheme which also included the previous observations about C V (Edlén & Löfstrand 1970). These energy levels are the part of critically analysed data base NIST (Kramida et al. 2015). From the theoretical perspectives, there exist quite a few atomic structure calculations of C V. Drake (1988) designed a theoretical unified method and reported very accurate level energies belonging to $n = 1$ and $n = 2$. In this unified method the effects of relativity were added as corrections to non-relativistic variational calculations. Vainshtein & Safronova (1985) incorporated relativistic and radiative effects in the perturbation theory for the calculations of He-like and Li-like systems. The relativistic configuration interaction calculations (Chen, Cheng & Johnson 1993; Cheng et al. 1994) and relativistic all order many body calculations (Plante, Johnson & Sapirstein 1994) were also employed for He-like ions including C V. Multiconfiguration Dirac Fock (MCDF) model (Dyall et al. 1989) and relativistic FAC (flexible atomic code) (Gu 2003) were used by Aggarwal et al. (2011) to get energy levels and transition parameters for C V. The theoretical energy levels, transitions rates and oscillator strengths are also compiled in CHIANTI data base (Del Zanna et al. 2015). In this data base these quantities are calculated with AUTOSTRUCTURE code (Badnell 2011) in which Breit–Pauli distorted wave approximation is implemented. Recently, Xie et al. (2012) carried out MCDHF (Grant 2007; Jönsson et al. 2007) calculations during their study of plasma effects on atomic structure of C V. In the present study, same MCDHF formalism have been adopted but with a larger configuration space of orbital and coupled with the Relativistic Configuration Interaction (RCI) to perform calculations which enabled us to get more accurate structure data. For this purpose we have utilized the package GRASP2K (Jönsson et al. 2013) which is the latest version of GRASP family of codes. The rest of the paper will proceed in the following way. The atomic structure, PI and PR computations are described in Section 2. In Section 3 the present MCDHF+RCI and DARC calculations are compared with available experimental and theoretical results. Finally we will briefly conclude our study in Section 4.

2 COMPUTATIONS

The underlined theory can be found in detail in Grant (2007), Jönsson et al. (2007) and Jönsson et al. (2013) which is recently described briefly by Bilal et al. (2017). In this section we outline some computational steps of atomic structure calculations of C IV. First we had taken non-relativistic configurations ($1s^2$, $1s2l$, $1s3l$, l = s, p, d) as multireference (MR) configurations for even and odd parity states. There were seven blocks of even and odd parities for J equal to 0–3. The MCDHF calculations were performed for the lowest 17 even and odd parity states simultaneously in the lowest order approximation using extended optimal level scheme and levels were given standard weights. The complete active space configuration expansion was generated by all possible excitations from MR to $4l$ layer (l = s, p, d, f). The MCDHF calculation was also performed for this stage by varying orbitals only in $n = 4$ layer and keeping the remaining fixed. This step was repeated for $n = 5, 6, 7$ layers of the correlation orbitals and for all layers, orbitals up to f were taken. Each time MCDHF calculation was followed by the RCI calculation by taking only Breit interaction, because for this simpler system of C V, QED effects had no influence on the accuracy. The RCI calculations had improved the mixing coefficients but the radial components (large and small) of target wavefunctions were remained unperturbed. The related transition parameters such as weighted oscillator strengths and transitions rates were calculated for electric and magnetic multipole transitions (E1, M2, E2, M1). We had derived another quantity dT proposed by Froese Fischer (2009) and Ekman, Godefroid & Hartman (2014) to indicate the consistency between length and velocity gauges and hence the accuracy of our results,

$$\mathrm{d}T = \frac{|A_l - A_v|}{\max(A_l, A_v)}, \tag{1}$$

where A_l and A_v are the transition rates in length and velocity forms, respectively.

For the calculations of PI cross-sections we had adopted similar Dirac R-matrix approach as described in Sardar et al. (2015). In PI process the final state was achieved either directly (non-resonant) or through some intermediate state (resonant). In this method the resonant passages of PI from the ground and excited states of C IV can be shown by following expressions

$$\begin{aligned} h\nu + 1s^2 2s(\mathrm{or}3s)\ (^2S_{1/2}) \rightarrow\ & [(1snln'l')(^2P_{1/2,3/2})] \\ & \downarrow \\ & 1snl + \bar{e}(kl'), \end{aligned} \tag{2}$$

$$\begin{aligned} h\nu + 1s^2 2p(\mathrm{or}3p)\ (^2P_{1/2,3/2}) \rightarrow\ & \begin{cases} (1snln'l') \\ (^2S_{1/2}, {}^2P_{1/2,3/2}, \\ {}^2D_{3/2,5/2}) \end{cases} \\ & \downarrow \\ & 1snl + \bar{e}(kl'), \end{aligned} \tag{3}$$

$$h\nu + 1s^2 3d\ (^2D_{3/2,5/2}) \rightarrow \begin{cases} (1snln'l') \\ (^2P_{1/2,3/2},\ ^2D_{3/2,5/2}, \\ ^2F_{5/2,7/2}) \end{cases} \downarrow \quad 1snl + \bar{e}(kl'). \tag{4}$$

The numerically determined radial wavefunctions from MCDHF calculation were input to DARC in a suitable format. To ensure the accuracy for the atomic structure calculations in the internal region of the R-matrix formalism, we had adopted model of 23 configurations ($1s^2$, $1snl$, 2s3s, 3s4s, 2p3p, 2p4p, 3p4p, nl^2, $n = 2$, 3, 4 and l = s, p, d, f) in which single and double excitations from ground state ($1s^2$) were taken. The lowest 17 target energy levels of C V arising from these configurations were used for the generations of scattering channels. The (N+1)-electron capture states (correlation functions) were constructed by the coupling of continuum electron states to the target states arising from these configurations. With the objective of delineating the resonance structure and well characterizing the PI cross-section and eigenphase profile, an appropriate energy step of 0.0001 eV (≈7 μRyd.) was taken. The boundary radius in R-matrix calculations was set at 8.4 au to envelope sufficient bound orbital of the target ion C V and the basis of 80 continuum orbitals per angular momentum was taken to span the entire energy range. The resonance positions in the PI cross-sections were determined to be where the change in the eigenphase sum ($\delta(E)$) was maximum. The following integral was evaluated to get the resonance strengths,

$$\bar{\sigma} = \int_{E_i}^{E_f} \sigma(E)\, \mathrm{d}E, \tag{5}$$

where the extension of resonances was delimited by the initial and final energies (E_i and E_f, respectively). The cross-sections for time inverse PR process of PI were then obtained from the principle of detailed balance (Chen 2008),

$$\sigma_{PR}(E) = \frac{\alpha^2}{4}\frac{g_i}{g_f}\frac{\omega^2}{E}\sigma_{PI}(E), \tag{6}$$

where E and ω are the energies of photoelectron and photon, respectively, α is the fine structure constant, g_i is the statistical weight of the recombined state (ground or metastable) of C IV and g_f is that of recombining state of C V. Equation (6) was applied to PI of ground state $1s^2 2s\ ^2S_{1/2}$ and metastable states $1s^2 2p\ ^2P_{1/2,3/2}$, $1s^2 3s\ ^2S_{1/2}$, $1s^2 3p\ ^2P_{1/2,3/2}$ and $1s^2 3d\ ^2D_{3/2,5/2}$, and then summed over all these contributions to get the PR cross-sections for $1s^2\ ^1S_0$ of C V. The PI and PR cross-sections belonging to KLL and KLM resonant regions were convoluted with a Gaussian with FWHM (full width at half-maximum) to make comparison with experimental observations of Müller et al. (2009) and Mannervik et al. (1997).

3 RESULTS AND DISCUSSIONS

Before presenting the PI and PR cross-sections, first we will discuss the results of our ab initio calculations for the atomic structure of C IV.

3.1 Energy levels, radiative rates of C V

In Table 1, we present the theoretical energies of the lowest 17 target states of C V from MCDHF+RCI calculations along with experimental values compiled in NIST (Kramida et al. 2015) data base and theoretical energy values from version 8.0 of continuously improving CHIANTI data base (Del Zanna et al. 2015). In order to make the comparison more comprehensive, some other theoretical published results (Xie et al. 2012; Aggarwal et al. 2011; Vainshtein & Safronova 1985) are also tabulated in Table 1. It is evident that our present target state energies are in better agreement with NIST values than any other theoretical results. The maximum deviation with the NIST values is only 0.002 per cent (53 cm^{-1}) for the level 1s2p ($^1P_1$). However, the average difference among our calculated values and NIST values is only 0.0005 per cent (12.29 cm^{-1}) which is remarkable by any standard. The energy levels from MCDHF calculations (Xie et al. 2012) but with different sets of active and correlation orbitals, also have better accuracy than other theoretical results (Aggarwal et al. 2011; Vainshtein & Safronova 1985). The maximum and average difference in their results from NIST is 0.005 per cent (113.82 cm^{-1}) and 0.002 per cent (63.87 cm^{-1}), respectively. Therefore, accompanying RCI calculations as adopted in our computational model clearly enhance the accuracy of target wavefunctions. The energy levels calculated by the perturbation theory (Vainshtein & Safronova 1985) are in good agreement with NIST but are less accurate than our calculated values. The accuracy levels of remaining two calculations from AUTOSTRUCTURE (CHIANTI) and FAC (Aggarwal et al. 2011) are not as high as those of our, Xie et al. (2012) or Vainshtein & Safronova (1985), however, they provide large-scale data and are within 0.03 and 0.27 per cent, respectively, with experiment. Moreover, the level ordering is very much sensitive to mixing from terms of same J (total angular momentum) value and parity and the inclusion of Breit interactions in RCI calculations. In our computations the exact experimental level ordering is achieved after layer by layer additions of correlation orbitals from $n = 4l$ to $7l$, l = s, p, d, f and subsequent RCI calculations. The level ordering presented in Table 1 for the other calculations, except for the level ordering of Vainshtein & Safronova (1985), is not same as the NIST level ordering. Even the accurate MCDHF calculations (Xie et al. 2012) have different level ordering for levels 4/5 (1s2p: $^3P_0/^3P_1$) and 10/11 (1s3p: $^3P_0/^3P_0$), this may be due to the missing Breit interaction in their calculations. This difference of level ordering occurs in AUTOSTRUCTURE and FAC calculations by CHIANTI and Aggarwal et al. (2011), respectively, which is possibly due to the limited mixing terms in their calculations.

In Table 2 we present the comparisons of some multipole (E1, M2, E2, M1) transitions energies and wavelengths of C V. For transition energies comparison, we have taken previous data from theoretical calculations of Xie et al. (2012), Cheng et al. (1994), Chen et al. (1993) and Drake (1988). The transition energies and wavelengths from NIST are also tabulated in Table 2 to make comparison with the experiment. The most of the wavelengths in the NIST data base are derived from known experimental upper and lower levels using Ritz principle, and these Ritz wavelengths are believed to be more accurate than observed wavelengths (Kramida et al. 2015). The indices for the upper and lower levels in these transitions are same as labelled in Table 1. The present transition energies are in excellent agreement with NIST with an average difference of 0.02 per cent. Particularly, our calculated X-ray lines are in remarkable agreement (within 0.0006 per cent) with observations. The present X-ray energy for $K_{\alpha 2}$ ($2^3P_1 \rightarrow 1^1S_0$) is in better agreement with NIST than other theoretical results (Drake 1988; Cheng et al. 1994). However, the Drake (1988) reported X-ray energy for $K_{\alpha 1}$ ($2^1P_1 \rightarrow 1^1S_0$) is more better than the present value. For the transition lines of UV spectrum ($2^3P_0 \rightarrow 2^3S_1$, $2^3P_1 \rightarrow 2^3S_1$, $2^3P_2 \rightarrow 2^3S_1$), the energy values from the theoretical work (Drake 1988; Chen et al. 1993) have more accuracy than our calculated values, nevertheless, our results for these lines are better than 0.13 per cent with observations. The EUV transition energies tabulated in Table 2 have an

Table 1. Comparison of target state energies for 17 levels with experimental (NIST) and theoretical results in cm^{-1}.

Index	Target states	Terms	NIST	MCDHF+RCI	MCDHF	Perturbation theory	CHIANTI	FAC	Per cent Err
1	$1s^2$	$^1S_0$	0	0	0	0	0	0	
2	1s2s	$^3S_1$	2411 271	2411 228	2411 302	2411 400	2410 835	2401 579	0.0018
3	1s2s	$^1S_0$	2455 026	2455 042	2455 125	2455 100	2453 333	2450 759	0.0007
4	1s2p	$^3P_1$	2455 157	2455 163	2455 180	2455 200	2453 189	2449 270	0.0002
5	1s2p	$^3P_0$	2455 170	2455 176	2455 088	2455 300	2453 090	2449 286	0.0003
6	1s2p	$^3P_2$	2455 293	2455 298	2455 362	2455 400	2453 390	2449 392	0.0002
7	1s2p	$^1P_1$	2483 373	2483 426	2483 487	2483 300	2483 600	2481 694	0.0021
8	1s3s	$^3S_1$	2839 574	2839 557	2839 640	2839 600	2838 636	2831 143	0.0006
9	1s3s	$^1S_0$	2851 180	2851 175	2851 266	2851 400	2851 397	2843 832	0.0002
10	1s3p	$^3P_1$	2851 406	2851 404	2851 470	2851 200	2850 675	2843 352	0.0001
11	1s3p	$^3P_0$	2851 408	2851 405	2851 470	2851 200	2850 646	2843 351	0.0001
12	1s3p	$^3P_2$	2851 446	2851 443	2851 443	2851 300	2850 735	2843 392	0.0001
13	1s3d	$^3D_1$	2857 306	2857 298	2857 369	2857 400	2856 748	2848 105	0.0003
14	1s3d	$^3D_2$	2857 307	2857 297	2857 378	2857 400	2856 759	2848 105	0.0003
15	1s3d	$^3D_3$	2857 318	2857 308	2857 391	2857 500	2856 776	2848 116	0.0003
16	1s3d	$^1D_2$	2857 530	2857 531	2857 609	2857 600	2857 012	2848 473	0.0000
17	1s3p	$^1P_1$	2859 369	2859 390	2859 470	2859 400	2859 569	2852 272	0.0007

NIST: Experimental energy values; MCDHF+RCI: present theoretical energy levels; MCDHF: theoretical calculations of Xie et al. (2012); perturbation theory: theoretical values for energy levels (Vainshtein & Safronova 1985); CHIANTI: AUTOSTRUCTURE calculations of energy levels (Del Zanna et al. 2015); FAC: theoretical energy levels (Aggarwal et al. 2011) and per cent Err: the per cent error between the present and NIST energies.

excellent accuracy of 0.02 per cent with NIST values. Similarly, the wavelengths related to these transitions particularly the X-ray transitions are indicating the remarkable agreement between the present theory and the experiment.

In Table 3 we list more structure data of C V target ion in terms of oscillator strengths and transition rates for E1 transitions in length form only. The velocity form can be taken into account by another quantity dT (Froese Fischer 2009; Ekman et al. 2014) which is the estimation of discrepancy between length and velocity form. The complete form of this table and data for M2, E2 and M1 transitions are available in the online version of the paper. Although, the dT value for each transition rate A (even for weak transitions) is showing consistency between two forms but average value of dT (0.0006) is more likely to confirm the authenticity of the target wavefunctions. For comparison we also present transition data from CHIANTI data base and other available theoretical calculations of Morton & Drake (2016), Xie et al. (2012), Aggarwal et al. (2011), Porquet & Dubau (2000) and Cann & Thakkar (1992). The oscillator strengths for the majority of the transitions in the present calculations, are within 3 per cent margin with the CHIANTI values. The theoretical reported oscillator strengths of Cann & Thakkar (1992) are tabulated in NIST data base and the present oscillator strengths for the transitions (7-1, 17-1, 7-3, 17-3, 17-9) are in strong agreement with them. Generally, our oscillator strengths for strong E1 transitions lines agree very well with the previous theoretical results (Morton & Drake 2016; Xie et al. 2012).

In brief, this excellent agreement between theory and experiment does indeed show the quality and accuracy of the target wavefunctions.

3.2 PI of C IV and PR of C V

As discussed earlier, the present RCI calculations (Breit interaction) improve only the mixing coefficients and radial wavefunctions remain the same as from the MCDHF calculations. These unperturbed radial wavefunctions are input to DARC for the structure calculations of the target ion C V. In order to maintain the accuracy in the N-electron target states we have adopted an atomic model of 23 configurations which have yielded very accurate target states energies with an average difference of only 0.07 per cent with the NIST. Moreover, the agreement of our calculated ionization energies of ground and excited states with experimental values supports our adopted approach of the calculations of PI and PR cross-sections. In Table 4 we present the ionization energies of the ground state and some excited states of C IV along with the experimental values of these states from NIST data base. The ionization energy of the ground state 2s $^2S_{1/2}$ is better than ≈0.03 per cent with NIST value. The maximum deviation from NIST is ≈0.1 per cent for the states 2p $^2P_{1/2,\,3/2}$ but all states differ by only 0.06 per cent on the average with the experiment, indicating the accuracy in the present calculations.

In the present calculations of PI cross-sections, the excitations from K-shell to $n = 2$, 3, 4 are taken as expansion of the target ion C V wavefunctions which give rise to important KLL and KLM resonances in the PI and PR cross-sections. These resonances follow the auto-ionization path to reach the final state of target ion and free electron. There is smooth decreasing pattern manifesting direct PI process between KLL and KLM resonances because there is an energy rise between the target states belonging to $n = 2$ and $n = 3$. In Fig. 1 we present DARC calculations for total (a) and partial (b) PI cross-sections, respectively, for the ground state $1s^22s\ ^2S_{1/2}$. The accuracy of the present DARC calculations is well reflected by a very good agreement between two gauges (length and velocity) of PI cross-sections. The background of the PI cross-sections in both total and partial PI process is same over a long energy range and is monotonically decreasing. Similarly, the resonance structures for both total and partial cross-sections are same but at high energies the total PI cross-sections exhibit more resonances than the partial cross-sections. This is mainly because in partial PI, the target ion has only ground level in final state and therefore the total PI cross-sections involve more auto-ionization channels than partial PI cross-sections at high energies. Similarly in Figs 2(a) and 2(b) the PI cross-sections for two excited states $1s^22p^2\ P_{1/2,\,3/2}$ of C IV also have consistency in both gauges (length and velocity). In this case the background and resonant PI cross-sections for these states have almost similar patterns and both states differ by very small amount

Table 2. Comparison of the present transition energies ΔE in cm^{-1} and wavelengths λ in Å for the selective multipole transitions in C V with the experiment and other theoretical calculations. Level numbers associated with the lower and upper states are same as in Table 1.

Transitions	Type	$\Delta E_{Exp.}$	$\Delta E_{Present}$	$\Delta E_{Unified\ theory}$	ΔE_{others}	λ_{NIST}	$\lambda_{Present}$
2-1	M1	2411 271.20	2411 227.54		2411 301.71[a]	41.47	41.47
4-1	E1	2455 157.3	2455 163.34	2455 178.84	2455 256.05[b]	40.73	40.73
6-1	M2	2455 293.20	2455 298.18		2455 362.40[a]	40.73	40.73
7-1	E1	2483 372.8	2483 425.80	2483 400.63	2483 475.69[b]	40.27	40.27
10-1	E1	2851 406.0	2851 403.80		2851 469.64[a]		35.07
12-1	M2	2851 443.49	2851 446.00		2851 443.32[a]		35.07
14-1	E2	2857 306.50	2857 297.42		2857 378.07[a]		35.00
16-1	E2	2857 530.30	2857 531.06		2857 608.53[a]	35.00	34.99
17-1	E1	2859 368.6	2859 390.02		2859 469.72[a]	34.97	34.97
4-2	E1	43 866.1	43 935.79	43 886.22	43 886.20[c]	2277.92	2276.04
5-2	E1	43 899.0	43 948.77	43 898.96	43 898.70[c]	2277.25	2275.37
6-2	E1	44 021.6	44 070.63	44 021.94	44 022.00[c]	2270.91	2269.08
7-2	E1	72 101.6	72 198.25		72 184.91[a]		1385.07
10-2	E1	440 134.8	440 176.25		440 167.93[a]	227.20	227.18
11-2	E1	440 136.3	440 177.78		440 167.95[a]	227.20	227.18
12-2	E1	440 174.8	440 215.95		440 141.61[a]	227.18	227.16
17-2	E1	448 097.4	448 162.47		448 168.01[a]		223.13
10-3	E1	396 380.5	396 362.13		396 344.28[a]		252.29
17-3	E1	404 343.1	404 348.36		404 344.36[a]	247.32	247.31
5-4	M1	13.0	12.98	12.70	12.50[c]		
8-4	E1	384 416.5	384 393.64		384 459.44[a]	260.14	260.15
9-4	E1	396 022.7	396 011.40		396 085.31[a]		252.52
13-4	E1	402 148.4	402 133.46		402 189.06[a]	248.66	248.67
14-4	E1	402 149.2	402 134.09		402 197.84[a]	248.66	248.67
16-4	E1	402 373.0	402 367.73		402 428.30[a]		248.53
8-6	E1	384 280.6	384 258.80		384 277.27[a]	260.23	260.24
13-6	E1	402 012.5	401 998.62		402 006.89[a]	248.75	248.76
14-6	E1	402 013.3	401 999.25		402 015.67[a]	248.75	248.76
15-6	E1	402 024.8	402 010.23		402 028.84[a]	248.74	248.75
16-6	E1	402 237.1	402 232.89		402 246.13[a]		248.61
8-7	E1	356 201.0	356 131.18		356 153.05[a]		280.79
9-7	E1	367 807.2	367 748.94		367 778.92[a]	271.88	271.92
13-7	E1	373 932.9	373 871.00		373 882.67[a]		267.47
14-7	E1	373 933.7	373 871.63		373 891.45[a]		267.47
16-7	E1	374 157.5	374 105.27		374 121.91[a]	267.27	267.30

Exp.: Experimental values compiled by NIST; Present: MCDHF+RCI calculations in this work; Unified theory: theoretical values reported in Drake (1988).

[a]MCDHF calculations (Xie et al. 2012).

[b]Relativistic CI calculations (Cheng et al. 1994).

[c]Relativistic CI calculations (Chen et al. 1993).

in ionization energies. The complete data for PI cross-sections of ground state ($1s^2 2s\ ^2S_{1/2}$) and excited states ($1s^2 2p\ ^2P_{1/2,\,3/2}$, $1s^2 3s\ ^2S_{1/2}$, $1s^2 3p\ ^2P_{1/2,\,3/2}$, $1s^2 3d\ ^2D_{3/2,\,5/2}$) of C IV are available in the online version of the paper.

When the energy of the incoming photon approaches near K-edge, the inner-shell excitations occur which lead to the doubly excited intermediate states before emission of 2s electron of C IV. The PI following these intermediate states appear as resonance at the smooth decaying cross-section of PI of outer electron of C IV. The experimental PI cross-sections for three electron doubly excited intermediate states [1s(2s2p) ^{3}P] ^{2}P, [(1s(2s2p) ^{1}P] ^{2}P (KLL), [(1s2s) ^{3}S3p] ^{2}P (KLM) arising from excitation processes 1s → 2p, 3p are reported by Müller et al. (2009). These PI cross-sections have experimental uncertainties of 20 and 40 per cent for KLL and KLM resonances, respectively. The energy resolutions in their experiment are 46 and 121 meV for KLL and KLM resonances, respectively. In order to check the validity of our calculations, the present PI cross-sections are convoluted with the same Gaussian of FWHM as the experimental resolutions to make direct comparison with experiment. In Fig. 3(a)–(c) we compare present DARC calculations with available ALS experimental results of Müller et al. (2009). We find very good agreement between our theoretical results and experiment for the resonance line profiles of these resonances. The present PI cross-sections for these resonances agree very well with experiment within the experimental uncertainties. As can be seen from Table 5 where we compare the present resonant energies and strengths with the previous experimental and theoretical results. The resonance energies for [1s(2s2p) ^{3}P] ^{2}P and [(1s(2s2p) ^{1}P] ^{2}P are in excellent agreement with both the experiments [ALS (Müller et al. 2009) and CRYRING (Mannervik et al. 1997)] as compared to the R-matrix calculations of Müller et al. (2009) and Saddle point method (SPM) of Mannervik et al. (1997). The more accurate value for the energy splitting of these two resonances, than the previous theoretical calculations further establishes the accuracy of the present work. However, for the third resonance the resonance energy from these theoretical calculations is in better agreement than the present result where the deviations from ALS and CRYRING are 0.4 and 0.3 eV, respectively. It should be noted that in Table 5 our calculated inte-

Table 3. Present oscillator strengths gf_P and transitions rates A_P in s^{-1} for electric dipole transitions in C V compared with other theoretical calculations. Level numbers associated with the lower and upper states are same as in Table 1. The notation $x \pm b$ means $x \times 10^{\pm b}$.

Transitions	gf_P	$gf_{CHIANTI}$	gf_{others}	A_P	$A_{CHIANTI}$	A_{others}	dT
4-1	2.096−05	1.434−05	2.118−05[a]	2.809+07	1.919+07	2.837+07[a]	0.0226
7-1	6.462−01	6.726−01	6.471−01[b]	8.862+11	9.225+11	8.863+11[d]	0.0001
10-1	4.539−06	3.387−06	5.047−06[c]	8.205+06	6.120+06	6.939+06[e]	0.0230
17-1	1.409−01	1.528−01	1.405−01[b]	2.562+11	2.779+11	2.566+11[d]	0.0002
4-2	1.320−01	1.299−01	4.551−02[c]	5.666+07	5.182+07	5.655+07[e]	0.0003
5-2	4.402−02	4.320−02	1.517−02[c]	5.671+07	5.145+07	5.616+07[e]	0.0005
6-2	2.208−01	2.175−01	2.207−01[d]	5.720+07	5.256+07	5.735+07[e]	0.0003
7-2	6.836−06		2.197−06[c]	7.923+03		8.012+03[c]	0.0597
10-2	3.156−01	3.087−01	1.018−01[c]	1.359+10	1.328+10	1.375+10[e]	0.0001
11-2	1.052−01	1.029−01	3.394−02[c]	1.359+10	1.328+10	1.376+10[e]	0.0000
12-2	5.254−01	5.146−01	1.695−01[c]	1.358+10	1.328+10	1.374+10[e]	0.0001
17-2	7.862−06		2.236−06[c]	3.511+05		2.898+05[e]	0.0056
7-3	9.348−02		9.308−02[b]	1.674+07		1.308+07[c]	0.0019
10-3	1.353−05			4.727+05		4.013+05[e]	0.0041
17-3	3.526−01	3.592−01	3.516−01[b]	1.282+10	1.318+10	1.457+10[e]	0.0008
17-9	1.607−01		1.617−01[b]	2.412+06		1.751+06[c]	0.0036
8-4	6.800−02	6.156−02	2.152−02[c]	2.234+09	2.033+09	2.129+09[e]	0.0015
9-4	1.207−06		4.043−07[c]	1.262+05		1.271+05[c]	0.0066
13-4	4.918−01	4.927−01	1.645−01[c]	1.768+10		1.761+10[e]	0.0004
14-4	1.470+00	1.475+00	4.923−01[c]	3.172+10	3.204+10	3.168+10[c]	0.0004
16-4	5.145−03	3.239−03	1.229−03[c]	1.111+08	7.045+07	7.917+07[c]	0.0008
8-6	1.136−01	1.025−01	2.156−02[c]	3.729+09	3.383+09	3.557+09[e]	0.0015
13-6	3.279−02	3.283−02	6.581−03[c]	1.178+09		1.176+09[c]	0.0004
14-6	4.899−01	4.911−01	9.842−02[c]	1.056+10	1.066+10	1.055+10[c]	0.0004
15-6	2.755+00	2.758+00	5.529−01[c]	4.242+10	4.276+10	4.233+10[c]	0.0004
16-6	2.099−03	1.362−03	3.091−04[c]	4.530+07	2.959+07	3.317+07[c]	0.0013
8-7	2.845−06		8.733−07[c]	8.024+04		7.297+04[c]	0.0171
9-7	6.339−02	7.107−02	2.105−02[b]	5.719+09	6.413+09	5.646+09[e]	0.0039
13-7	1.551−05		4.814−06[c]	4.821+05		4.434+05[c]	0.0069
14-7	7.779−03	5.117−03	1.901−03[c]	1.451+08	9.505+07	1.050+08[c]	0.0010
16-7	2.105+00	2.137+00	7.045−01[b]	3.931+10	3.976+10	3.953+10[c]	0.0006
10-8	2.214−01	2.258−01	7.509−02[c]	6.908+06	7.278+06	7.187+06[c]	0.0008
11-8	7.382−02	7.509−02	2.504−02[c]	6.912+06	7.225+06	7.191+06[c]	0.0003
12-8	3.703−01	3.782−01	3.704−01[d]	6.980+06	7.386+06	6.978+06[d]	0.0007
17-8	1.213−05		3.767−06[c]	1.061+03		1.055+03[c]	0.0339

Notes. [a]Morton & Drake (2016).
[b]Cann & Thakkar (1992).
[c]Aggarwal et al. (2011).
[d]Xie et al. (2012).
[e]Porquet & Dubau (2000).

Table 4. Ionization energies of the lowest levels of C IV in eV.

Levels	Terms	This work	NIST
2s	$^2S_{1/2}$	64.47	64.49
2p	$^2P_{1/2}$	56.44	56.50
2p	$^2P_{3/2}$	56.42	56.49
3s	$^2S_{1/2}$	26.94	26.95
3p	$^2P_{1/2}$	24.79	24.81
3p	$^2P_{3/2}$	24.79	24.81
3d	$^2D_{3/2}$	24.21	24.21
3d	$^2D_{5/2}$	24.21	24.21

grated cross-sections for individual resonances are consistent with radiatively damped R-matrix calculations of Müller et al. (2009). It should also be mentioned that although our resonance strength is slightly lower than previous theoretical results for [(1s2s) ^{3}S3p] ^{2}P, there is large discrepancy between theories and ALS experiment for this KLM resonance state. Additionally, in ALS experiment, the accuracy in the energies and cross-sections in the KLM region is linearly extrapolated from the KLL energy region which makes the experimental results for [(1s2s) ^{3}S3p] ^{2}P less accurate than those for [1s(2s2p) ^{3}P] ^{2}P and [(1s(2s2p) ^{1}P] ^{2}P.

The PR cross-sections from present calculations are shown in Fig. 4(a) and (b). These PR cross-sections in the KLL and KLM energy regions are consistent with those plotted in figs 1(a), 2(a) and fig. 1 of references Zhao et al. (2000) and Zhang, Nahar & Pradhan (1998), respectively. The small differences of peak values for KLM resonances, between our results and Zhang et al. (1998), cannot be attributed to the missing of RD in our calculations. The larger energy step in the calculations of Zhang et al. (1998) leads to underestimation of the cross-sections, which is also pointed out by Zhao et al. (2000). For direct comparison with the experimental PR cross-sections (Mannervik et al. 1997), the present PR cross-sections are convoluted with a Gaussian of the same FWHM as the experimental resolution of 0.57 eV (Pradhan & Zhang 1997). Fig. 5(a) illustrates the present convoluted PR cross-section as a function of electron energy in KLL resonance region. All

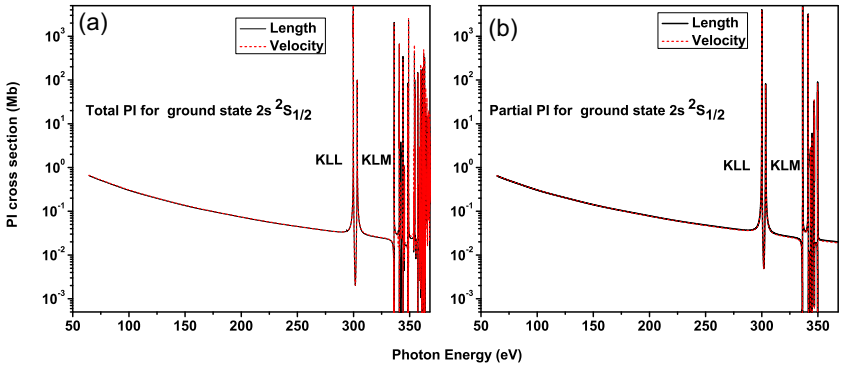

Figure 1. PI cross-sections of C IV with the present DARC calculations for the ground state ($1s^2 2s\ ^2S_{1/2}$) in length and velocity gauges: (a) total PI cross-sections and (b) partial PI cross-sections in which after PI the target ion is left only in ground state, KLL and KLM resonances are marked in both cases.

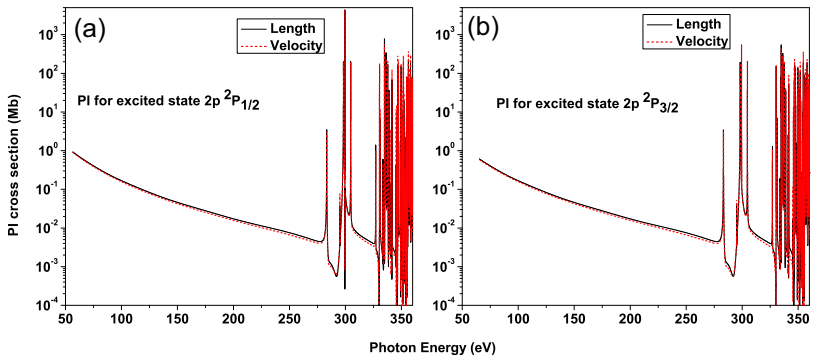

Figure 2. Length and velocity forms of PI cross-sections of C IV for two excited states with the present DARC calculations [(a)$1s^2 2p\ ^2P_{1/2}$ and (b) $1s^2 2p\ ^2P_{3/2}$].

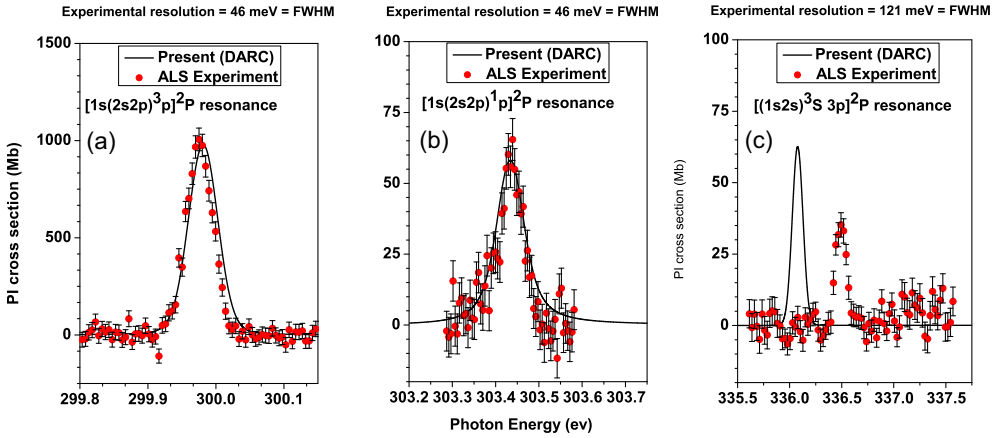

Figure 3. PI cross-sections for the ground state ($1s^2 2s\ ^2S_{1/2}$) of C IV compared with experimental (Müller et al. 2009) PI cross-sections for three resonances (a) (1s(2s2p) ^{3}P) ^{2}P, (b) (1s(2s2p) ^{1}P) ^{2}P and (c) ((1s2s) ^{3}S 3p) ^{2}P. PI cross-section from DARC are convoluted with Gaussian of FWHM of 46 meV for KLL resonances and of 121 meV for KLM resonance. The solid red circles with error bars in all panels are the experimental data provided by Dr. Alfred Müller.

five resonances appear in the present PR cross-sections which are observed experimentally by Mannervik et al. (1997) (Fig. 5b) and predicted theoretically by Zhao et al. (2000), Pradhan & Zhang (1997) and Zhang et al. (1998). The relatively low intensity resonance $1s2s^2\ ^2S$ at energy about 227 eV can only be possible when it mixes with the state $1s2p^2\ ^2S$ which is the intermediate doubly excited state in the PR process from ground state $1s^2\ ^1S_{1/2}$ of C V to the final metastable state $1s^2 2p\ ^2P_{1/2,\,3/2}$ of C IV. In addition to these five resonances there exist another resonance, $1s2p^2\ ^2P$ at the energy about 243 eV which is the demonstration of fully relativistic approach based on *jj* coupling adopted in the present calculations. The PI or PR through such type of doubly excited state is not possible in LS coupling scheme (Zhao et al. 2000), because no even parity final (N+1)-electron state is available. We note that this particular resonance in our calculations is more pronounced as compared to that shown in fig. 2(c) of reference Pradhan & Zhang (1997). The underestimation of this narrow resonance is again, because of the larger energy step in their relativistic treatment of PR.

Similarly, the convoluted PR cross-sections shown in Fig. 5(c) in the KLM region produce the observed resonances (Mannervik et al. 1997) shown in Fig. 5(d). Nine resonances out of 12 exper-

Table 5. Comparison of resonance energies E_{res} (eV) and resonance strengths $\bar{\sigma}$ (Mb eV) from present calculations with the experimental and theoretical published results.

Resonance		Experiment		Theory			
		ALS	CRYRING	DARC	Breit–Pauli R-matrix	LS coupling R-matrix	SPM
[1s(2s2p) ^{3}P] ^{2}P	E_{res}	299.98 ± 0.03	299.98 ± 0.05	299.97	299.99	299.94	299.99
	$\bar{\sigma}$	53 ± 2	52.6 ± 0.8	55.49	53.30	54.4	
[(1s(2s2p) ^{1}P] ^{2}P	E_{res}	303.44 ± 0.03	303.48 ± 0.05	303.43	303.50	303.43	303.46
	$\bar{\sigma}$	4.5 ± 0.7	6.5 ± 0.4	5.49	5.60	5.80	
[(1s2s) ^{3}S3p] ^{2}P	E_{res}	336.50 ± 0.10	336.36 ± 0.05	336.08	336.39	336.33	336.39
	$\bar{\sigma}$	4.5 ± 0.9	7.0 ± 0.4	8.17	8.60	8.50	
Energy splitting	ΔE	3.461 ± 0.004	3.50	3.462	3.509	3.499	3.465

ALS: Experimental results from Müller et al. (2009); CRYRING: experimental values from Mannervik et al. (1997); DARC: present theoretical values; Breit–Pauli R-matrix: theoretical values from Müller et al. (2009); LS coupling R-matrix: theoretical values from Müller et al. (2009); SPM: theoretical values from Saddle point method of Mannervik et al. (1997).

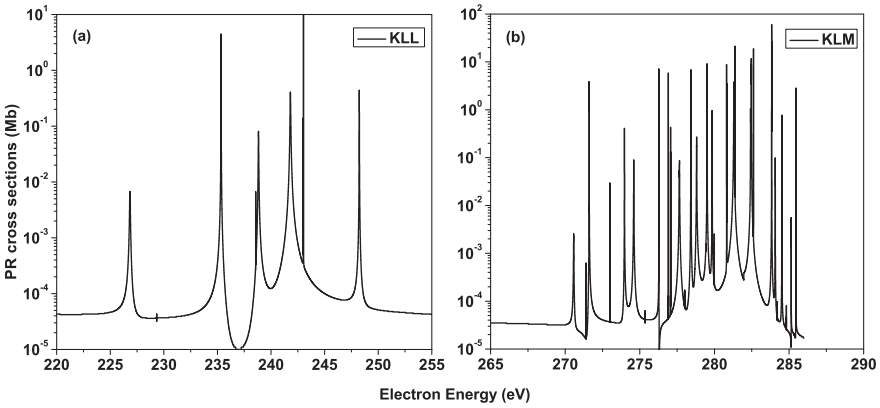

Figure 4. Present PR cross-sections in KLL (a) and KLM (b) energy regions.

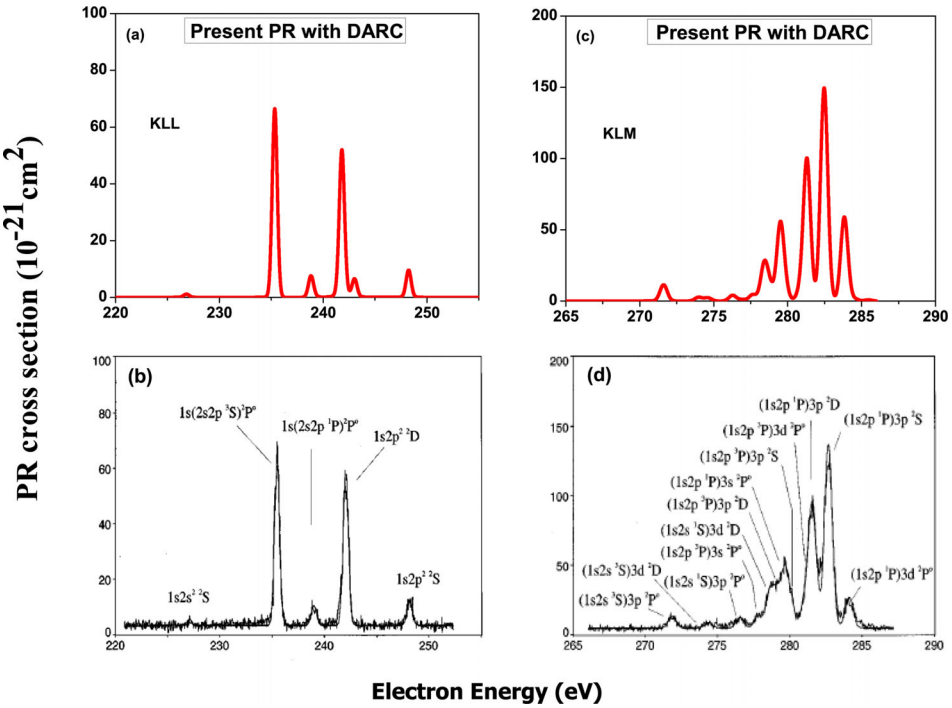

Figure 5. Comparison of the present PR cross-sections of C V with the experimental PR cross-sections, (a) DARC calculations in the KLL resonance region; (b) Mannervik et al. (1997); (c) DARC calculations in KLM resonance region and (d) Mannervik et al. (1997). The present PR cross-sections are convoluted with a Gaussian with FWHM of 0.57 eV. The panels (b) and (d) are reprinted after taking licence from American Physical Society and permission from Mannervik et al. (1997).

Table 6. Comparison of present integrated PR cross-sections (10^{-21} cm^2 eV) with the available experimental and theoretical results.

	Experiment		Theory		
Resonance	CRYRING	TSR	DARC	Kilgus	NRHF[a]
$1s2s^2\ ^2S$	0.7(0.2)		0.76	1.23	
$1s(2s2p\ ^3P)\ ^2P^o$	39.3(6)	39.3(9)	40.61	44.13	39.05
$1s(2s2p\ ^1P)\ ^2P^o$	4.9(3)	6.1(6)	4.89	5.36	13.18
$1s2p^2\ ^2D$	37.2(6)	34.5(8)	33.90	37.85	42.18
$1s2p^2\ ^2P$		3.1(6)	4.24		
$1s2p^2\ ^2S$	5.9(3)	5.6(5)	5.99	7.58	8.41
$(1s2s\ ^3S)3p\ ^2P^o$	5.7(3)		6.94		7.69
$(1s2s\ ^3S)3d\ ^2D$	2.5(3)		3.02		
$(1s2s\ ^1S)3p\ ^2P^o$	5.1(3)		2.79		2.60
$(1s2p\ ^3P)3s\ ^2P^o$	6.0(3)		4.68		31.29
$(1s2s\ ^1S)3d\ ^2D$	16.2(6)		18.21		
$(1s2p\ ^3P)3p\ ^2D$	16.2(7)				11.28
$(1s2p\ ^1P)3s\ ^2P^o$	27.1(7)		37.72		11.22
$(1s2p\ ^3P)3p\ ^2S$	9.5(6)				2.75
$(1s2p\ ^3P)3d\ ^2P^o$	12.8(6)				7.80
$(1s2p\ ^1p)3p\ ^2D$	60.0(9)		64.49		21.77
$(1s2p\ ^1p)3p\ ^2S$	89.0(10)		91.92		4.31
$(1s2p\ ^1p)3d\ ^2P^o$	15.0(4)		36.73		1.35

CRYRING: Experimental values from Mannervik et al. (1997); TSR: experimental values from Kilgus et al. (1993); DARC: present theoretical values; Kilgus: theoretical values from Kilgus et al. (1993); NRHF: theoretical values from Bellantone & Hahn (1989).
[a]In addition to these resonant states, Bellantone & Hahn (1989) report two other KLM resonant states $(1s2p\ ^1P)3d\ ^2F$ and $(1s2p\ ^3P)3d\ ^2F$ with integrated cross-sections 24.63×10^{-21} and 61.91×10^{-21} cm^2 eV, respectively.

imentally observed resonances are easily noticeable while other 3 resonances $(1s2p\ ^3P)3p\ ^2D$, $(1s2p\ ^3P)3p\ ^2S$ and $(1s2p\ ^3P)3d\ ^2P$ are lying on the other relatively strong resonances due to convolution process. We have found that the major contribution for the peak marked with $(1s2p\ ^1P)3p\ ^2S$ in Fig. 5(d), comes from PR cross-sections for the recombined states $1s^23d\ ^2D_{3/2,\,5/2}$. Therefore, as can be seen from equation (4), this particular peak can be marked with resonant state $(1s2p\ ^1P)3d\ ^2F$ (Zhao et al. 2000). Our calculated PR cross-sections have very good match in position and line profile with the experimental PR cross-sections as well as with the radiatively damped theoretical PR cross-sections shown in figs 2(b) and (g) of Zhao et al. (2000) and Pradhan & Zhang (1997), respectively. It should be noted that our calculated PR cross-sections are in better agreement with the experiment as compared to those from undamped perturbative and close coupling calculations of Zhao et al. (2000). However, for the resonant state $(1s2p^1P)3d^2P$ near 284 eV, the present PR cross-section is overestimated as compared to the damped PR cross-section of Zhao et al. (2000) due to the missing of RD in our calculations. In Table 6 the integrated PR cross-sections for KLL and KLM resonances are tabulated to make quantitative comparison of present calculations with the previous experiments and theories. As compared to non-relativistic Hartree Fock procedure (NRHF) of Bellantone & Hahn (1989), our calculated integrated cross-sections have an overall very good agreement with the CRYRING experiment and are within the experimental uncertainties. We note that the sum of present integrated cross-sections of the nine KLM resonances is $\approx 267 \times 10^{-21}$ cm^2 eV which is the same value as that obtained by integrating the unconvolved PR cross-sections over the entire KLM energy range. Therefore, these nine KLM resonances include the effects of resonant states $(1s2p\ ^3P)3p\ ^2D$, $(1s2p\ ^3P)3p\ ^2S$ and $(1s2p\ ^3P)3d\ ^2P$. On the other hand, the totals of integrated cross-sections of KLM resonances from previous theoretical results of Kilgus et al. (1993) and Bellantone & Hahn (1989) are 274.9×10^{-21} and 188.6×10^{-21} cm^2 eV, respectively. It should be noted that the sum of integrated cross-sections of KLM resonances of Bellantone & Hahn (1989) includes the contributions from $(1s2p\ ^1P)3d\ ^2F$ (24.63×10^{-21} cm^2 eV) and $(1s2p\ ^3P)3d\ ^2F$ (24.63×10^{-21} cm^2 eV) resonant states. Finally, as compared to previous theories, we find good agreement of our calculated collective KLM integrated cross-section with the experimental values of CRYRING (265×10^{-21} cm^2 eV) (Mannervik et al. 1997) and Test Storage Ring (TSR) (260×10^{-21} cm^2 eV) (Kilgus et al. 1993), respectively.

4 CONCLUSION

In summary, we have carried out state of the art MCDHF+RCI calculations for the atomic structure parameters of C V followed by Dirac R-matrix PI calculations for C IV. Remarkable agreement between experiment and the present theoretical results was achieved for energy states, transition energies and wavelengths of the transitions in the fine structure levels of C V. The related oscillator strengths and transition rates were found to be consistent with other theoretical models. Our computational model for determining the required parameters of C V enabled us to achieve this high level of accuracy, and we believe our data to be very useful in diagnostics of solar plasma and analysing X-ray spectra originating from astronomical objects like AGNs, X-rays binaries etc.

Our PI cross-sections concorded with the experimental PI cross-sections of high resolution (Müller et al. 2009) at three important resonant states $(1s(2s2p)\ ^3P)\ ^2P$, $(1s(2s2p)\ ^1P)\ ^2P$ and $((1s2s)\ ^3S3p)\ ^2P$. Moreover, the derived PR cross-sections from PI cross-sections were found to be in good agreement with the experiments (Kilgus et al. 1993; Mannervik et al. 1997) in both KLL and KLM energy regions. Besides experiments, the consistency with the previous theoretical results with different approaches made the present PI and PR cross-sections reliable. The effects of RD can be excluded in the present study of PI and PR cross-sections of C IV and C V, respectively, except for the resonance state $(1s2p^1P)3d^2P$. Our PI and PR data are expected to be very useful for astronomical objects where the photoabsorption lines of X-rays are important.

ACKNOWLEDGEMENTS

This work is supported by the National Natural Science Foundation of China (Grant Nos. U1332204, U1732133 and 11320101003) and the National Key Research and Development Program of China (Grant Nos. 2017YFA0303500 and 2017YFA0402300). The authors are grateful to Dr. Alfred Müller for providing the experimental data of PI cross-sections.

REFERENCES

Aggarwal K. M., Kato T., Keenan F. P., Murakami I., 2011, Phys. Scr., 83, 015302
Badnell N. R., 2011, Comput. Phys. Commun., 182, 1528
Bellantone R., Hahn Y., 1989, Phys. Rev. A, 40, 6913
Berrington K. A., Eissner W., Norrington P. H., 1995, Comput. Phys. Commun., 92, 290
Bilal M., Beerwerth R., Volotka A. V. P., Fritzsche S., 2017, MNRAS, 469, 4620
Cann N. M., Thakkar A. J., 1992, Phys. Rev. A, 46, 5397
Chang J. J., 1977, J. Phys. B: At. Mol. Phys., 10, 3195
Chen G. X., 2008, Phys. Rev. A, 77, 022703
Chen M. H., Cheng K. T., Johnson W. R., 1993, Phys. Rev. A, 47, 3692
Cheng K. T., Chen M. H., Johnson W. R., Sapirstein J., 1994, Phys. Rev. A, 50, 247
Cooksey K. L., Thom C., Prochaska J. X., Chen H. W., 2010, ApJ, 708, 868
Del Zanna G., Dere K. P., Young P. R., Landi E., Mason H. E., 2015, A&A, 582, A56
Dere K. P., Landi E., Young P. R., Del Zanna G., 2001, ApJS, 134, 331
Drake G. W., 1988, Can. J. Phys., 66, 586
Dyall K. G., Grant I. P., Johnson C. T., Parpia F. A., Plummer E. P., 1989, Comput. Phys. Commun., 55, 424
Edlén B., Löfstrand B., 1970, J. Phys. B: At. Mol. Phys., 3, 1380
Ekman J., Godefroid M. R., Hartman H., 2014, Atoms, 2, 215
Engström L., Bengtsson P., Jupén C., Westerlind M., 1992, J. Phys. B, 25, 2459
Ferland G. J., Korista K. T., Verner D. A., Ferguson J. W., Kingdon J. B., Verner E. M., 1998, PASP, 110, 761
Froese Fischer C., 2009, Phys. Scr., T134, 014019
Grant I. P., 2007, Relativistic Quantum Theory of Atoms and Molecules. Springer, New York
Gu M. F., 2003, ApJ, 582, 1241
Jannitti E., Nicilosi P., Villoresi P., Xianping F., 1995, Phys. Rev. A, 51, 314
Jönsson P., He X., Froese Fischer C., Grant I. P., 2007, Comput. Phys. Commun., 177, 597
Jönsson P., Gaigalas G., Bieroé J., Froese Fischer C., Grant I. P., 2013, Comput. Phys. Commun., 184, 2197
Kallman T. R., Palmeri P., 2007 Rev. Mod. Phys., 79, 79
Kilgus G., Habs D., Schwalm D., Wolf A., Schuch R., Badnell N. R., 1993, Phys. Rev. A, 47, 4859
Kramida A., Ralchenko Yu., Reader J., NIST ASD Team, 2015, NIST Atomic Spectra Database (ver. 5.3) [Online]. Available at: http://physics.nist.gov/asd
Landi E., Alexander R. L., Gruesbeck J. R., Gilbert J. A., Lepri S. T., Manchester W. B., Zurbuchen T. H., 2012, ApJ, 744, 100
Mannervik S. Asp S., Bröstrom. L., DeWitt D. R., Lidberg J., Schuch R., 1997, Phys. Rev. A, 55, 1810
Morton D. C., Drake G. W. F., 2016 J. Phys. B: At. Mol. Phys., 49, 234002
Müller A. et al., 2009 J. Phys. B: At. Mol. Phys. 42, 235602
Nahar S. N., Pradhan A. K., Zhang H. L., 2000, ApJS, 131, 375
Norrington P. H., Grant I. P., 1981, J. Phys. B: At. Mol. Phys., 14, L261
Osakabe M. et al., 2014, Plasma Phys. Control. Fusion, 56, 095011
Plante D. R., Johnson W. R., Sapirstein J., 1994, Phys. Rev. A, 49, 3519
Porquet D., Dubau J., 2000, A&AS, 143, 495
Pradhan A. K., Zhang H. L., 1997, J. Phys. B: At. Mol. Phys., 30, L571
Robicheaux F., Gorezycea T. W., Griffen D. C., Pindzola M. S., Badnell N. R., 1995, Phys. Rev. A, 52, 1319
Sardar S., Bilal M., Nazir R. T., Bari M. A., Hannan A., Nasim M. H., 2015, MNRAS, 450, 1631
Scully S. W. J. et al, 2006, J. Phys. B: At. Mol. Phys., 39, 3957
Sofia U. J., Cardelli J. A., Guerin K. P., Mayer D. M., 1997, ApJ, 482, L105
Vainshtein L. A., Safronova U. I., 1985, Phys. Scr., 31, 519
Xie L. Y., Wang J. G., Janev R. K., Qu Y. Z., Dong C. Z., 2012, Eur. Phys. J. D. 66, 125
Zhang H. L., Nahar S. N., Pradhan A. K., 1997, J. Phys. B: At. Mol. Phys., 32, 1459
Zhao L. B., Ichihara A., Shirai T., 2000, Phys. Rev. A, 62, 022706

SUPPORTING INFORMATION

Supplementary data are available at *MNRAS* online.

Please note: Oxford University Press is not responsible for the content or functionality of any supporting materials supplied by the authors. Any queries (other than missing material) should be directed to the corresponding author for the article.

This paper has been typeset from a TEX/LATEX file prepared by the author.